Journal of Materials Chemistry A

Accepted Manuscript

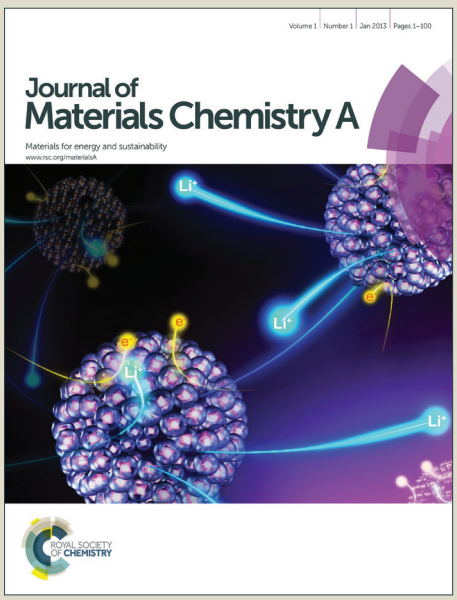

ROYAL SOCIETY OF CHEMISTRY

www.rsc.org/materialsA

Journal Name

RSCPublishing

ARTICLE

One-step Hydrothermal Synthesis of $NiCo_2S_4$-rGO as an Efficient Electrocatalyst for Oxygen Reduction Reaction

Cite this: DOI: 10.1039/x0xx00000x

Received 00th January 2012,
Accepted 00th January 2012

DOI: 10.1039/x0xx00000x

www.rsc.org/

Jianghong Wu, Shuo Dou, Anli Shen, Xin Wang, Zhaoling Ma, Canbin Ouyang, Shuangyin Wang*

In this work, for the first time, we have developed a one-step hydrothermal method to synthesize a hybrid material consisting of $NiCo_2S_4$ nanocrystals grown on reduced graphene oxide as an efficient nonprecious electrocatalyst for oxygen reduction reaction (ORR) in alkaline medium. Our synthetic process here is quite simple, straightforward and environment benign. In comparison with rGO, $NiCo_2O_4$-rGO, and commercial Pt/C, $NiCo_2S_4$-rGO shows significantly enhanced catalytic activity over rGO and $NiCo_2O_4$-rGO, and close reduction activity but much superior methanol tolerance and better durability to commercial Pt/C catalyst. The half wave potential ($E_{1/2}$) for $NiCo_2S_4$-rGO hybrid is only about 62 mV more negative than that of the commercial Pt/C catalyst but 81 mV more positive than $NiCo_2O_4$-rGO, 116 mV than rGO. The superior performance for $NiCo_2S_4$-rGO is presumably attributed to a combination effect of mixed valence in transition metals composites favorable for O_2 to be absorbed/reduced and a synergetic effect resulted from $NiCo_2S_4$ and rGO. The advantages over $NiCo_2O_4$-rGO might be ascribed to the inverse spinel crystal structure of $NiCo_2S_4$, its relative higher conductivity, and that Na_2S serves both as S source and reducing agent facilitating increasing the hybrid catalytic activity.

1. Introduction

Exploring high efficient and durable electrocatalysts at low cost for the oxygen reduction reaction (ORR) in fuel cells or metal-air battery to replace precious-metal ones such as platinum (and its alloy) has triggered extensive research interests.[1] Catalysts for ORR are the key part for the development of renewable energy technologies. Although Pt and its alloy remain the most efficient catalyst, its scarcity in nature leads to high cost in practical application, and it often suffers from declining activity, low tolerance to methanol which hinder the further development of fuel cell technologies. Until now, alternatives based on non-precious metals and their oxides or complex,[1-4] metal free materials such as heteroatom-doped / surface modified graphene or carbon nanotubes[5-9] have been intensively investigated. Among these alternatives, first row transition metal (Co, Mn, Ni, Fe, Cu, etc.) chalcogenides, such as oxides,[10-13] sulfides[14] have drawn vast attention due to their low cost, high electrocatalytic activity towards ORR. Carbon-based materials like graphene or carbon nanotube have high electrical conductivity, large surface area, usually bringing enhanced electrocatalytic properties to their hybrid and composite with other metal-based materials.[10] Indeed, carbon supported transition metal chalcogenides like Mn_3O_4-graphene/carbon nanotube,[3, 15] Co-O, Co-S binary composite[10, 14, 16, 17] have been reported showing superior electrocatalytic activity and stability. Combined with their abundance in nature, first row transition metal chalcogenides or supported on carbon-based materials have become one of the most promising electrocatalysts for ORR. Besides binary composite, ternary metal chalcogenides with a spinel structure such as $NiCo_2O_4$, $MnCo_2O_4$ and $NiCo_2S_4$ have shown advanced catalytic activity and stability for the ORR over their binary counterpart.[17-19] It has been studied that the advance of spinel structure for electrocatalytic activities is attributed to its octahedral sites occupied by electrocatalytic active metal ions[18, 20, 21]. Recently, $NiCo_2S_4$ grown on carbon support has been shown a comparable catalytic activity for ORR in the alkaline medium[18, 22] and has been proved that the excellent electrocatalytic property is resulted from the unique d-electronic configuration of Co(III) at the surface of $NiCo_2S_4$[18]. Though continuous research efforts have been undertaken to develop ternary metal chalcogenides with a spinel structure, this progress is still moving quite slowly. Until now, Zhang *et al.* reported synthesis of $NiCo_2S_4$-N/S co-doped rGO (reduced graphene oxide) hybrid based on two step solvethermal method, which exhibited high ORR activity with good stability in alkaline solutions[22]. But the catalysts still suffer low activity compared with commercial Pt/C and as to the synthetic method is limited in organic solvent or high temperature[18, 22], new strategies to develop transition metal chalcogenides catalysts are still desirable.

Here, we reported a facile method based on a one-step hydrothermal method to synthesize a hybrid material consisting of $NiCo_2S_4$ nanocrystals grown on reduced graphene oxide (rGO) with lower onset and peak potential for ORR, wherein aqueous solution was used instead of organic solvent at relatively lower reaction temperature. In the meanwhile, Na_2S serves both as S source and reductant[23], which might facilitate graphene oxide being reduced more completely during hydrothermal treatment.

Experimental

Catalysts preparation

The graphene oxide (GO) was prepared by a modified Hummers method.[24] In a typical synthesis, 0.5 mL $Ni(OAc)_2$•$6H_2O$ (0.11 M) and 0.5 mL $Co(OAc)_2$•$6H_2O$ (0.22 M) aqueous solution were added into 20 mL GO aqueous solution (1 mg/mL) under continuous magnetic stirring for 1 hour to form an uniform suspension (The mass loading of $NiCo_2S_4$ is 45wt%). After that, 10 mL Na_2S (0.088 M) aqueous solution was added, following a sudden color change from brown to black. After stirring for another 1 hour, the mixture was transferred to an autoclave (50 mL) and the hydrothermal reaction was carried out at 180 °C for 12 h. The resulted products were obtained by filtration, washed with deionized water for several times and collected by freeze drying for further characterization. rGO and $NiCo_2O_4$-rGO were prepared through the same procedure except for not adding of Ni^{2+} and Co^{2+} source or Na_2S but NH_4OH. CoS-rGO and NiS-rGO were made with the same procedure except for changing the ratio of Co (or Ni) and S to 1:1. To change the mass loading of $NiCo_2S_4$, the volume of $Ni(OAc)_2$•$6H_2O$ (0.11 M) and $Co(OAc)_2$•$6H_2O$ (0.22 M) were controlled to 0.105 mL for 15wt% and 0.895 mL for 60wt%.

Materials characterization

The microstructure of $NiCo_2S_4$-rGO was characterized by a transmission electron microscope (TEM，JEOL-2100F). The crystal structure was detected by a RigakuB/Max 2500 X-ray diffractometer using Cu Kα as the radiation source (λ = 1.5406). X-ray photoelectron spectroscopic (XPS) measurements were performed on an ESCALAB 250Xi using a monochromic Al X-ray source (200 W, 20 eV).

Electrochemical measurement

The electrochemical tests were carried out on an electrochemical workstation (CHI 760E, CH Instrument, USA) using a three-electrode cell. Glassy carbon (GC) with catalyst coated on, a platinum mesh and a saturated calomel electrode (SCE) were used as the working electrode, the counter electrode and the reference electrode, respectively. The catalyst ink was prepared as follows: 4 mg of the catalyst was dispersed 2 ml ethanol within 20 μL of 5 wt % Nafion and then treated by sonication for 10 minutes to form a homogenous ink. 20 μL of the catalyst ink was dropped onto the surface of GC electrode with 4 mm in diameter (the catalysts loading was 0.32 mg cm^{-2} for all catalysts). The ORR performance was first evaluated by cyclic voltammetry (CV) in N_2 and O_2-saturated 0.1 M KOH at room temperature, with a sweep rate of 10 mV s^{-1}. Linear sweep voltammetry (LSV) was carried out under constant O_2 gas flow, with a sweep rate of 10 mV s^{-1} in the potential range of 0 to -0.8 V vs SCE. For the measurement of linear sweep voltammetry (LSV), rotating ring-disk electrode (RRDE) was employed with a rotation speed of 1600 rpm in 0.1 M KOH solution saturated with O_2. For comparison test of durability, both $NiCo_2S_4$-rGO and commercial Pt/C were examined by continuous CV scanning from 0 to -0.8 V at a scan rate of 100 mV s^{-1} for 2000 cycles in 0.1 M KOH and the LSV curves were recorded before and after 2000 cycles in 0.1 M KOH solution saturated with O_2. For comparison test of methanol tolerance, both $NiCo_2S_4$-rGO and commercial Pt/C were conducted by CV scanning from 0 to -1 V at a scan rate of 10 mV s^{-1} in 0.1 M KOH and 0.1 M KOH+1M methanol solution respectively, with a rotation speed of 1600 rpm. For all the figures, the SCE reference were converted into RHE following equation reported by Liang YY, *et al.*:[1]

$$E(RHE)=E(SCE)+0.99V\ (0.1M\ KOH)$$

To test the chemical stability of $NiCo_2S_4$ as an electrocatalyst in alkaline medium, XRD measurements were conducted on carbon supported $NiCo_2S_4$ before and after 2000 CV cycles in 0.1 M KOH solution, shown in Fig. S5.

2. Results and discussion

Co^{2+} and Ni^{2+} ion were anchored on negatively charged GO sheets and formed into $NiCo_2S_4$ once Na_2S was added. During the hydrothermal process, $NiCo_2S_4$ nanocrystals (NCs) were formed and GO sheets turned into rGO. This synthesis process is similar to the formation of rGO sheets decorated with other nanoparticles, as reported previously.[11] Fig. 1a) shows representative TEM images of the as-synthesized $NiCo_2S_4$-rGO, as it shows, $NiCo_2S_4$ NCs were attached to the rGO without obvious aggregation, suggesting that the functional groups like hydroxyl (-CO) and carboxyl (-COOH) on the GO sheets successfully serve as anchors for $NiCo_2S_4$ NCs growing[25] and also efficiently prevent their aggregation. The diameters are distributed in the range of 25-35 nm, as revealed in the histogram inserted in Fig. 1b). A high-resolution TEM image (HRTEM) in Fig. 1b) reveals the crystalline structure of $NiCo_2S_4$ NCs and the d-spacing of 0.283 corresponds to the distance of the (311) planes. The powder X-ray diffraction pattern shown in Fig. 1c) was used to reveal the crystal structure of the as synthesized materials. The peaks are relatively broadening but well indexed as pure $NiCo_2S_4$ with a cubic phase (JCPDS card No. 20–0782), suggesting nanocrystalized $NiCo_2S_4$ were successfully formed during hydrothermal process. Besides, there is a more widen diffraction peak (002) around 24°; this is attributed to rGO[4], indicating GO has been successfully reduced to rGO during our hydrothermal process.

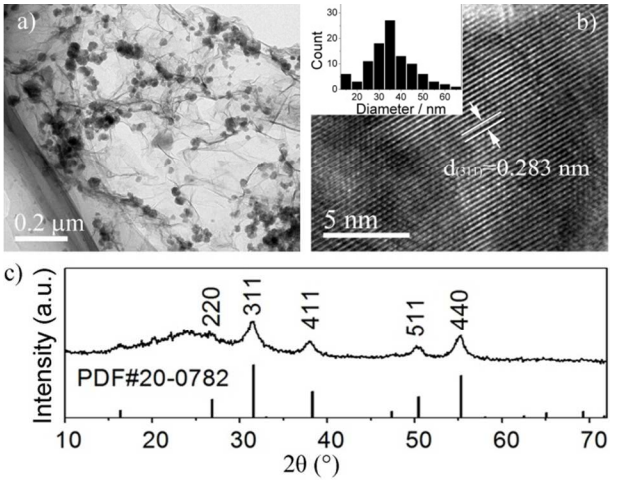

Fig. 1 a) TEM, b) HRTEM images (Inset: diameter distribution of $NiCo_2S_4$ NCs) and c) XRD pattern of as-synthesized $NiCo_2S_4$-rGO

The X-ray photoelectron spectroscopy (XPS) analysis shown in Fig. 2 gives the detailed information about the composition and surface electronic structure of the as-synthesized $NiCo_2S_4$-rGO. As expected, the survey spectra (Fig. 2a)) further confirms the existence of Ni, Co, S and C elements in the as-synthesized products. The spectrum for Ni 2p is shown in Fig. 2b), as it reveals, the main peak at 853.1 eV is indexed to Ni^{2+}, and the peak at 855.4 eV is attributed to Ni^{3+},[26] indicating the existence of both Ni^{2+} and Ni^{3+} valence in the products. For Co 2p (Fig. 2c)), the peaks at 778.6 eV and 780.2 eV correspond to Co^{3+}; 780.2 eV and 794.3 eV to Co^{2+}.[27, 28] For S 2p (Fig. 2d)), 161.7 eV and 163.6 eV are indexed to metal-sulfur bonds, while 162.8 eV corresponds to S^{2-} in low coordination and 164.7 eV is indexed to thiophenic-S (aromatic C-S-C), indicating S was

somehow doped in graphene, which might be benefit for its improvement in electrochemical property.[27, 29] It is clearly that adding excessive Na_2S aroused a possibility of the simultaneous incorporation of S atoms into the rGO during the formation of $NiCo_2S_4$.

To examine the electrocatalytic performance of the as-prepared $NiCo_2S_4$-rGO for ORR, the cyclic voltammograms (CVs) measurement was employed in O_2- or N_2- saturated 0.1 M KOH solutions at a sweep rate of 10 mV s^{-1}. As shown in Fig. 3a), the reduction reaction was processing in the presence of oxygen but not nitrogen. The onset ORR potential was around 0.88 V vs. RHE, which was derived from where 10% of the current value at the peak potential is reached[19], and it's reduction peak is at 0.79 V. For comparison, the CVs of rGO and $NiCo_2O_4$-rGO were given in Fig. 3b) and Fig. S1. It is clearly seen that our $NiCo_2S_4$-rGO showed significantly superior catalytic activity in terms of onset and peak potentials over rGO and $NiCo_2O_4$-rGO. These values of our $NiCo_2S_4$-rGO are even lower than the one in previous work[22] and the comparison with other literatures can be found in Table S1.

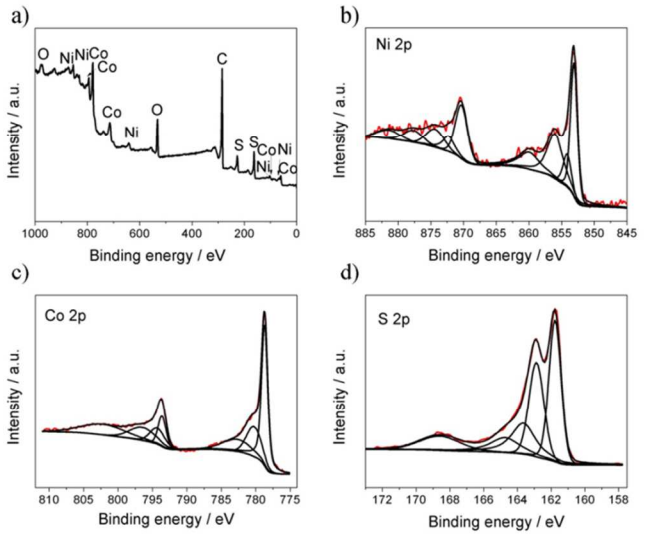

Fig. 2 a) XPS survey spectra of $NiCo_2S_4$-rGO and b), c) and d) high resolution Ni 2p, Co 2p and S 2p spectra, respectively.

To further reveal the ORR kinetic of $NiCo_2S_4$-rGO, rotating disk electrode (RDE) voltammetry (linear-sweep voltammetry, LSV) was performed in O_2-saturated 0.1M KOH solution at a scan rate of 10 mV s^{-1}. As shown in Fig. 3c), $NiCo_2S_4$-rGO electrode shows a one-step pathway, indicating a four-electron reaction. Obviously, the limiting current density increases with rotation rate increasing. At 1600 rpm, the onset potential is much close to that of commercial 20 wt% Pt/C (Johnson Matthey Corp.) and more positive than $NiCo_2O_4$-rGO as revealed in Fig. 4. The half wave potential ($E_{1/2}$) for $NiCo_2S_4$-rGO hybrid is about 0.733 V vs. RHE, which is only about 62 mV more negative compared with that of the commercial Pt/C catalyst but 81 mV more positive than $NiCo_2O_4$-rGO (0.652 V vs. RHE), 116 mV than rGO (0.617 V vs. RHE, Fig. S2). The excellent performance of $NiCo_2S_4$-rGO might be attributed to a combination effect of mixed valence in transition metals composites which have been favorable for O_2 to be absorbed and reduced,[26] and a synergetic effect resulted from $NiCo_2S_4$ and rGO.[1] The superior performance of $NiCo_2S_4$-rGO over $NiCo_2O_4$-rGO is probably attributed to the inverse spinel crystal structure of $NiCo_2S_4$ which contains more octahedral catalytic active sites of Co^{3+} [18]and its relative higher conductivity.[30]

The transferred electron numbers per O_2 involved in the oxygen reduction can be calculated by the Koutechy-Levich equation as given below:

$$\frac{1}{j} = \frac{1}{j_k} + \frac{1}{B\omega^{0.5}}$$

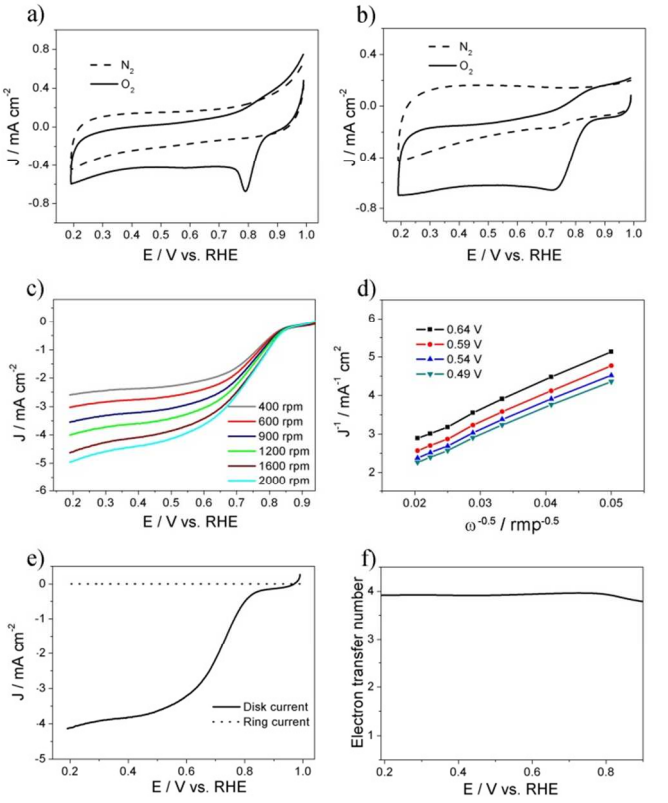

Fig. 3 Cyclic voltammetry (CV) curves of ORR on a) $NiCo_2S_4$-rGO and b) $NiCo_2O_4$-rGO in N_2- and O_2-saturated 0.1 M KOH solutions at a scan rate of 10 mV s^{-1}; c) LSV curves at various different rotation rates for oxygen reduction in an O_2-saturated 0.1M KOH solution; d) K-L plots of ORR; e) ORR on the RRDE in an O_2-saturated 0.1 M KOH solution; f) the electron transfer number (n) of $NiCo_2S_4$-rGO at different potentials derived from the corresponding RRDE data in Fig. 3e).

Where j_k is the kinetic current and ω is the electrode rotating rate. B could be determined from the slope of the K-L plots (Figure 3d)) based on the Levich equation as follows:

$$B = 0.2nF(D_{O_2})^{2/3}\nu^{-1/6}C_{O_2}$$

Where n corresponds to the number of transferred electrons per oxygen molecule, F is the Faraday constant (F = 96485 C mol^{-1}), $\boldsymbol{D_{O_2}}$ is the diffusion coefficient of O_2 in 0.1 M KOH (1.9 $\times 10^{-5}$ cm^2 s^{-1}), υ is the kinetic viscosity (0.01 cm^2 s^{-1}), and $\boldsymbol{C_{O_2}}$ is the bulk concentration of O_2 (1.2 $\times$ 10^{-6} mol cm^{-3}). The constant 0.2 is adopted when the rotation speed is expressed in rpm[31].

The fitting lines in Fig. 3d) are nearly linear and parallel, suggesting similar electron transfer numbers for ORR at different potentials and first-order reaction kinetics in relation to the concentration of

dissolved O_2.[32] The electron transfer number (n) from the slopes of K-L plots is calculated to be 3.64-3.93 throughout the potential range of 0.64 to 0.49V vs. RHE, suggesting $NiCo_2S_4$-rGO processed a four electron ORR pathway. For further determination, the ORR pathway of $NiCo_2S_4$-rGO was also examined through rotating ring-disk electrode (RRDE) measurements. The disk and ring currents were shown in Fig. 3e) and the electron transfer number (n) at various potential were calculated and plotted in Fig. 3f). As it can be seen, the ORR pathway catalyzed by $NiCo_2S_4$-rGO is dominated by a four-electron process. The average electron transfer number was 3.93 over the potential range of 0.19V to 0.79 V vs. RHE. This is in accord with the result obtained from the Koutecky-Levich plots based on RDE measurements, suggesting the ORR catalyzed by $NiCo_2S_4$-rGO is a 4e reduction reaction.

In order to investigate the effect of $NiCo_2S_4$ mass loading on ORR catalytic activity, we compared the electrochemical performances of $NiCo_2S_4$-rGO with different $NiCo_2S_4$ mass loading of 15wt%, 45wt% and 60wt% by LSV, as revealed in Fig. S3. It can be observed that the mass loading of 15% shows very low activity which goes higher when the mass loading increased. 60wt% shows almost the same catalytic activity as 45wt% in terms of onset potential. The higher $NiCo_2S_4$ content would cause abundant $NiCo_2S_4$ nanoparticles detached from rGO,[10] so there is no obvious improvement on ORR catalytic activity when the $NiCo_2S_4$ content is higher than 45wt%. We also explored the different electrochemical performances between binary (e.g. CoS and NiS) and ternary NiCo composites. As revealed in Fig. S4, $NiCo_2S_4$-rGO shows higher catalytic activity over either NiS-rGO or CoS-rGO. The ORR onset potential of NiCo2S4-rGO is 0.078 V and 0.058 V vs. RHE more positive than NiS-rGO and CoS-rGO respectively. This observation is consistent with the previous reports that ternary transition metals chalcogenides are advantageous than their binary counterpart on ORR catalytic activity.[12, 22, 33]

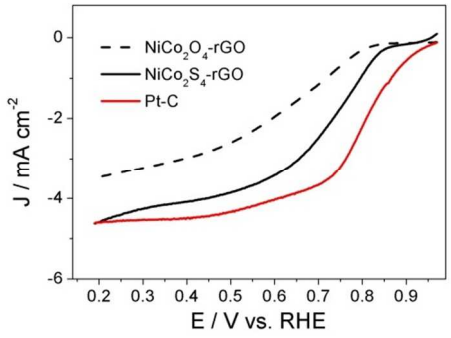

Fig. 4 RDE curves of Pt-C 20%, $NiCo_2S_4$-rGO and $NiCo_2O_4$-rGO in O_2-saturated 0.1 M KOH at 1600 rpm with a sweep rate of 10 mV s^{-1}.

Additionally, we accessed the durability of $NiCo_2S_4$-rGO and commercial Pt/C by cycling the catalysts between 0.99 and 0.19 V vs. RHE at 100 mV s^{-1}. After 2000 continuous cycles, the onset potential of ORR on Pt/C electrocatalysts shifted negatively by 157 mV, while $NiCo_2S_4$-rGO slightly shifted negatively only by 27 mV (Fig. 5a) and b)). This result clearly confirms that the stability of our $NiCo_2S_4$-rGO is much better than that of Pt/C electrocatalyst and the high durability of $NiCo_2S_4$-rGO could be inferred to the contribution of the heteroatom-doped graphene with stable structure.[22]

In the practical application of methanol fuel cells (DMFCs), ORR catalysts should be well tolerant to the methanol, but current Pt-based catalysts suffer methanol crossover effect. We therefore measured the CV curves in the potential range between 0.99 and -0.01 V vs. RHE at a scan rate of 10 mV s^{-1} in 0.1 M KOH within or without the presence of 1 M methanol and keep the electrode rotating at 1600 rpm. As expected, there is a dramatic decrease in the ORR activity of Pt/C (Fig. 5d)), while on the contrary, the CV curves were almost overlapped for $NiCo_2S_4$-rGO within or without the presence of 1 M methanol (Fig. 5c)). This observation indicates that $NiCo_2S_4$-rGO has excellent fuel selectivity towards ORR than the commercial Pt/C electrocatalyst.

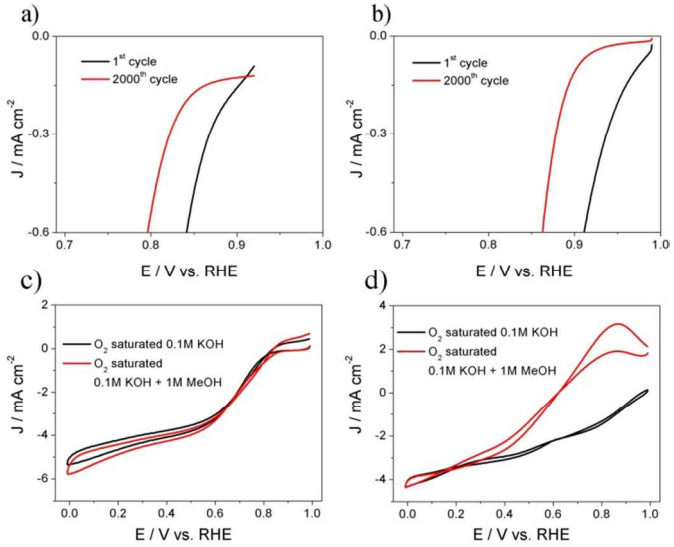

Fig. 5 RDE curves of a) $NiCo_2S_4$-rGO and b) Pt-C 20% in O_2-saturated 0.1 M KOH at 1600 rpm with a sweep rate of 10 mV s^{-1} before and after 2000 CV cycles. Cyclic voltammetry (CV) curves of ORR on c) $NiCo_2S_4$-rGO and d) Pt-C 20% at a rotating rate of 1600 rpm in oxygen-saturated 0.1m KOH solutions and 0.1m KOH + 1M methanol solutions at a scan rate of 10 mV s^{-1}.

Conclusions

$NiCo_2S_4$-rGO hybrid was synthesized by a facile one step hydrothermal method as an effective and low cost nonprecious electrocatalyst for oxygen reduction reaction (ORR) in the alkaline medium, where Na_2S serves as both S source and reductant. $NiCo_2S_4$-rGO shows excellent catalytic activity over rGO, NiS-rGO, CoS-rGO and $NiCo_2O_4$-rGO, and close reduction activity but much superior methanol tolerance and better durability to commercial Pt/C catalyst. The excellent performance of $NiCo_2S_4$-rGO might be a combination effect of mixed valence in transition metals composites which have been favorable for O_2 to be absorbed and reduced, and a synergetic effect resulted from $NiCo_2S_4$ and rGO. The superior performance of $NiCo_2S_4$-rGO over $NiCo_2O_4$-rGO is probably attributed to its relative higher conductivity and the inverse spinel crystal structure of $NiCo_2S_4$ with more octahedral catalytic active sites of Co^{3+}. Moreover, Na_2S serves both as S source and reducing agent facilitating the reduction of GO and aroused a possibility of the simultaneous incorporation of S atoms into the rGO, increasing its catalytic activity. This work demonstrated that transition metal

chalcogenides could be a promising electrocatalysts for ORR in the future application.

Acknowledgements

The authors acknowledge the support from the National Natural of Science Foundation of China (Grant No.: 51402100), the Youth 1000 Talent Program of China and China Postdoctoral Science Foundation Funded Project (No. 2014M552133). The authors would also like to thank Prof. Jiwu Huang, Prof. Gao Wang and Prof. Lanping Huang from Central South University for their assistance with XRD, XPS and TEM measurements.

Notes and references

State Key Laboratory of Chem/Bio-Sensing and Chemometrics, College of Chemistry and Chemical Engineering, Hunan University, Changsha, 410082, P. R. China.
*Corresponding author
E-mail: shuangyinwang@hnu.edu.cn

Electronic Supplementary Information (ESI) available: See
DOI: 10.1039/c000000x/

1. Y. Liang, Y. Li, H. Wang, J. Zhou, J. Wang, T. Regier and H. Dai, *Nat. Mater.*, 2011, **10**, 780.
2. Z.-S. Wu, S. Yang, Y. Sun, K. Parvez, X. Feng and K. Müllen, *J. Am. Chem. Soc.*, 2012, **134**, 9082.
3. J. Duan, Y. Zheng, S. Chen, Y. Tang, M. Jaroniec and S. Qiao, *Chem. Commun.*, 2013, **49**, 7705.
4. R. Huang, H. Ge, X. Lin, Y. Guo, R. Yuan, X. Fu and Z. Li, *RSC Adv.*, 2013, **3**, 1235.
5. S. Dou, A. Shen, L. Tao and S. Wang, *Chem. Commun.*, 2014, **50**, 10672.
6. A. Shen, Y. Zou, Q. Wang, R. A. W. Dryfe, X. Huang, S. Dou, L. Dai and S. Wang, *Angew. Chem. Int. Ed.*, 2014, **53**, 10804.
7. X. Wang, J. Wang, D. Wang, S. Dou, Z. Ma, J. Wu, L. Tao, A. Shen, C. Ouyang, Q. Liu and S. Wang, *Chem. Commun.*, 2014, **50**, 4839.
8. Y. Li, W. Zhou, H. Wang, L. Xie, Y. Liang, F. Wei, J.-C. Idrobo, S. J. Pennycook and H. Dai, *Nature Nanotechnology*, 2012, **7**, 394.
9. R. Ning, C. Ge, Q. Liu, J. Tian, A. M. Asiri, K. A. Alamry, C. M. Li and X. Sun, *Carbon*, 2014, **78**, 60.
10. Y. Y. Liang, H. L. Wang, P. Diao, W. Chang, G. S. Hong, Y. G. Li, M. Gong, L. M. Xie, J. G. Zhou, J. Wang, T. Z. Regier, F. Wei and H. J. Dai, *J. Am. Chem. Soc.*, 2012, **134**, 15849.
11. M. Wang, J. Huang, M. Wang, D. Zhang, W. Zhang, W. Li and J. Chen, *Electrochem. Commun.*, 2013, **34**, 299.
12. R. Ning, J. Q. Tian, A. M. Asiri, A. H. Qusti, A. O. Al-Youbi and X. P. Sun, *Langmuir*, 2013, **29**, 13146.
13. G. Zhang, B. Y. Xia, X. Wang and X. W. Lou, *Adv. Mater.*, 2014, **26**, 2408.
14. N. Mahmood, C. Z. Zhang, J. Jiang, F. Liu and Y. L. Hou, *Chem. Eur. J.*, 2013, **19**, 5183.
15. J. Feng, Y. Y. Liang, H. L. Wang, Y. G. Li, B. Zhang, J. G. Zhou, J. Wang, T. Regier and H. J. Dai, *Nano Res.*, 2012, **5**, 718.
16. L. Zhu, D. Susac, M. Teo, K. C. Wong, P. C. Wong, R. R. Parsons, D. Bizzotto, K. A. R. Mitchell and S. A. Campbell, *J. Catal.*, 2008, **258**, 235.
17. M. Hamdani, R. N. Singh and P. Chartier, *Int. J. Electrochem. Sci.*, 2010, **5**, 556.
18. Z. Zhang, X. Wang, G. Cui, A. Zhang, X. Zhou, H. Xu and L. Gu, *Nanoscale*, 2014, **6**, 3540.
19. L. Yu, L. Zhang, H. B. Wu and X. W. Lou, *Angew. Chem. Int. Ed.*, 2014, **53**, 3711.
20. J. Suntivich, H. A. Gasteiger, N. Yabuuchi, H. Nakanishi, J. B. Goodenough and Y. Shao-Horn, *Nat. Chem.*, 2011, **3**, 546.
21. J. Suntivich, K. J. May, H. A. Gasteiger, J. B. Goodenough and Y. Shao-Horn, *Science*, 2011, **334**, 1383.
22. Q. Liu, J. T. Jin and J. Y. Zhang, *ACS Appl. Mater. Interfaces*, 2013, **5**, 5002.
23. A. M. Schwartzberg, C. D. Grant, T. van Buuren and J. Z. Zhang, *J. Phys. Chem. C*, 2007, **111**, 8892.
24. W. S. Hummers Jr and R. E. Offeman, *J. Am. Chem. Soc.*, 1958, **80**, 1339.
25. S. Chen, J. Duan, W. Han and S. Z. Qiao, *Chem. Commun.*, 2014, **50**, 207.
26. M. Prabu, K. Ketpang and S. Shanmugam, *Nanoscale*, 2014, **6**, 3173.
27. J. Pu, T. Wang, H. Wang, Y. Tong, C. Lu, W. Kong and Z. Wang, *ChemPlusChem*, 2014, **79**, 577.
28. Y. Li, L. Cao, L. Qiao, M. Zhou, Y. Yang, P. Xiao and Y. Zhang, *J. Mater. Chem.*, 2014, **2**, 6540.
29. H. Chen, J. Jiang, L. Zhang, H. Wan, T. Qi and D. Xia, *Nanoscale*, 2013, **5**, 8879.
30. J. Xiao, L. Wan, S. Yang, F. Xiao and S. Wang, *Nano Lett.*, 2014, **14**, 831.
31. S. Wang, D. Yu and L. Dai, *J. Am. Chem. Soc.*, 2011, **133**, 5182.
32. M. Wang, W. Zhang, J. Wang, A. Minett, V. Lo, H. Liu and J. Chen, *J. Mater. Chem.*, 2013, **1**, 2391.
33. Y. Liang, H. Wang, J. Zhou, Y. Li, J. Wang, T. Regier and H. Dai, *J. Am. Chem. Soc.*, 2012, **134**, 3517.

Journal Name

RSCPublishing

ARTICLE

The table of contents entry

One step hydrothermal synthesized $NiCo_2S_4$-rGO hybrid shows excellent catalytic activity over $NiCo_2O_4$-rGO and close to Pt/C but with better stability.